CELL BIOLOGY

The Hippo pathway mediates Semaphorin signaling

Zhipeng Meng[1,2,3]*†, Fu-Long Li[1]†, Cao Fang[1], Benjamin Yeoman[4], Yunjiang Qiu[5,6], Ying Wang[2,3], Xiaomin Cai[2], Kimberly C. Lin[1], Di Yang[1], Min Luo[1,7], Vivian Fu[1], Xiaoxiao Ma[8], Yarui Diao[9], Filippo G. Giancotti[10,11], Bing Ren[5], Adam J. Engler[4], Kun-Liang Guan[1]*

Semaphorins were originally identified as axonal guidance molecules, but they also control processes such as vascular development and tumorigenesis. The downstream signaling cascades of Semaphorins in these biological processes remain unclear. Here, we show that the class 3 Semaphorins (SEMA3s) activate the Hippo pathway to attenuate tissue growth, angiogenesis, and tumorigenesis. *SEMA3B* restoration in lung cancer cells with *SEMA3B* loss of heterozygosity suppresses cancer cell growth via activating the core Hippo kinases LATS1/2 (large tumor suppressor kinase 1/2). Furthermore, SEMA3 also acts through LATS1/2 to inhibit angiogenesis. We identified p190RhoGAPs as essential partners of the SEMA3A receptor PlexinA in Hippo regulation. Upon SEMA3 treatment, PlexinA interacts with the pseudo–guanosine triphosphatase (GTPase) domain of p190RhoGAP and simultaneously recruits RND GTPases to activate p190RhoGAP, which then stimulates LATS1/2. Disease-associated etiological factors, such as genetic lesions and oscillatory shear, diminish Hippo pathway regulation by SEMA3. Our study thus discovers a critical role of Hippo signaling in mediating SEMA3 physiological function.

INTRODUCTION

Semaphorins are a large family of secreted or transmembrane proteins that were first identified as repulsive molecules of neural axonal growth cone (*1*–*3*). They were characterized by a common structure "SEMA" domain, which consists of approximately 500 amino acids and is essential for the interaction with their membrane receptors Plexins. Semaphorins are recognized as key regulators for cell morphology and mobility and play critical roles in the development of the neural system and cardiovascular system, as well as in other physiological processes. Recent studies have revealed differential roles of Semaphorins in various types of solid tumors, either tumor suppressing or tumor promoting depending on their transmembrane receptors and co-receptors in the biological contexts (*2*). Notably, class 3 Semaphorins (SEMA3s), which are a group of secreted Semaphorins that act through their receptors PlexinAs (PLXNAs) and co-receptors Neuropilins (NRPs), mainly function as tumor suppressors by inhibiting cancer cell growth, metastasis, and angiogenesis. Deletion or silencing of *SEMA3B* and *SEMA3F* genes has been observed in lung cancer, metastatic breast cancer, and renal carcinoma, among many other malignancies (*4*–*7*). However, despite the prominent roles of SEMA3s in various diseases, the downstream signaling pathway of SEMA3s is not fully understood.

[1]Department of Pharmacology and Moores Cancer Center, University of California, San Diego, La Jolla, CA 92093, USA. [2]Department of Molecular and Cellular Pharmacology, University of Miami Miller School of Medicine, Miami, FL 33136, USA. [3]Sylvester Comprehensive Cancer Center, Miami, FL 33136, USA. [4]Department of Bioengineering, University of California, San Diego, La Jolla, CA 92093, USA. [5]Ludwig Institute for Cancer Research, University of California, San Diego, La Jolla, CA 92093, USA. [6]Bioinformatics and Systems Biology Graduate Program, University of California, San Diego, La Jolla, CA 92093, USA. [7]State Key Laboratory of Oral Diseases, National Clinical Research Center for Oral Diseases, West China Hospital of Stomatology, Sichuan University, Chengdu, Sichuan, China. [8]Center for Immunotherapy and Precision Immuno-Oncology, Cleveland Clinic, Cleveland, OH 44195, USA. [9]Regeneration Next Initiative, Department of Cell Biology, Duke University School of Medicine, Durham, NC 27710, USA. [10]Department of Cancer Biology and David H. Koch Center for Applied Research of GU Cancers, The University of Texas MD Anderson Cancer Center, Houston, TX 77030, USA. [11]Herbert Irving Comprehensive Cancer Center and Department of Genetics, Vagelos College of Physicians and Surgeons, Columbia University, New York, NY 10033, USA.
*Corresponding author. Email: zxm282@med.miami.edu (Z.M.); kuguan@ucsd.edu (K.-L.G.)
†These authors contributed equally to this work.

The Hippo pathway, initially identified by a *Drosophila* mosaic screen for overgrowth phenotype, has been shown to play an important role in human cancers (*8*, *9*). The Hippo pathway kinases, mammalian STE20-like kinase 1/2 (MST1/2) and large tumor suppressor kinase 1/2 (LATS1/2), are well-established tumor suppressors. The kinase cascade of MST1/2 and LATS1/2 phosphorylates and inhibits YAP and TAZ, two transcriptional coactivators that promote tissue growth and regeneration through binding to the transcriptional enhanced associate domain family transcription factors (*10*). Activation of YAP/TAZ, in most cases due to inactivation of the Hippo kinase cascade, allows terminally differentiated cells to exit from quiescence and enter the cell cycle, mainly through initiating growth-promoting transcriptomes that relieve the constraints of cell-cell contact and cell–extracellular matrix adhesion and alter cellular responses to nutrient and hormone signals (*11*, *12*). Aberrant activation of YAP/TAZ alone is sufficient to drive the neoplastic transformation of cells in many scenarios, and elevation of YAP/TAZ is frequently observed in cancer (*8*, *9*). Moreover, the Hippo pathway has been established as one of the commonly altered signaling pathways in human cancer based on the recent The Cancer Genome Atlas (TCGA) data (*13*). However, one critical knowledge gap is how the Hippo pathway activity is maintained by physiological signals to restrict tissue overgrowth during tissue development and injury repair.

Here, we connected the Hippo pathway to SEMA3 through a signaling cascade from the module of PLXNA/p190RhoGAP/RND–guanosine triphosphatase (GTPase) to Hippo kinases MST1/2 and mitogen-activated protein kinase kinase kinase kinase (MAP4Ks). By controlling the YAP/TAZ-mediated transcriptome, SEMA3 restricts cell growth, angiogenesis, and tumorigenesis. We thus uncovered a long-sought downstream effector of SEMA3 and a previously unknown physiological signal for Hippo pathway regulation.

RESULTS

SEMA3 activates the Hippo signaling and inhibits YAP/TAZ activities via its receptor PLXNA

YAP and TAZ are mainly regulated by LATS1/2-dependent phosphorylation, which inhibits YAP/TAZ by promoting their cytoplasmic

localization and degradation (*10*). In the search for physiological factors that modulate the activity of YAP/TAZ, we found that SEMA3 could induce YAP/TAZ phosphorylation. Treatment with recombinant human SEMA3A (rSEMA3A) proteins or SEMA3A-conditioned medium, which was prepared from human embryonic kidney (HEK) 293A cells overexpressing human SEMA3A (fig. S1A), induced phosphorylation of YAP/TAZ in glioblastoma cell lines U87-MG and U373-MG, as well as HEK293A cells (Fig. 1A and fig. S1B). This was likely due to activation of the Hippo pathway because mutation of the LATS recognition sites abolished SEMA3A-induced YAP phosphorylation (fig. S1C). Moreover, phosphorylation of the LATS hydrophobic motif (HM), a marker for LATS kinase activity, was strongly induced by SEMA3A (Fig. 1A). Consequently, the mRNA level of YAP/TAZ target genes (*CTGF*, *CYR61*, and *ANKRD1*) was inhibited by the rSEMA3A treatment in both U87-MG and HEK293A cells (Fig. 1B). Furthermore, our RNA sequencing (RNA-seq) analyses of SEMA3-treated U87-MG cells revealed that SEMA3A regulated a myriad of known YAP/TAZ signature genes (Fig. 1C and fig. S1D) (*11*, *12*). Many SEMA3-regulated pathways or biological processes predicted by Gene Ontology analysis, such as cell morphogenesis and cell division (fig. S1E), are also regulated by the Hippo pathway as described previously (*14*, *15*).

To understand the mechanisms by which SEMA3A represses YAP/TAZ activities, we next determined whether the SEMA3 effects on YAP/TAZ activities required its transmembrane receptors PLXNAs. We generated PLXNA1/2/3 triple knockout (tKO) cell lines by CRISPR-Cas9 (fig. S1, F and G) and found that deletion of PLXNA1/2/3 abolished the SEMA3-induced phosphorylation of LATS and YAP/TAZ (Fig. 1D). Phosphorylation of YAP/TAZ is known to inactivate YAP/TAZ by inducing cytoplasmic localization (*10*). Consistently, SEMA3A induced cytoplasmic translocation of YAP/TAZ in the wild-type (WT) cells, but this effect was blocked in PLXNA1/2/3 tKO cells (Fig. 1E and fig. S2A). NRP1/2 are co-receptors for SEMA3 and work together with PLXNAs to relay SEMA3 signals. Particularly, NRP1/2 are involved in SEMA3-mediated tumor cell growth inhibition (*1*). Therefore, we generated NRP1/2 double

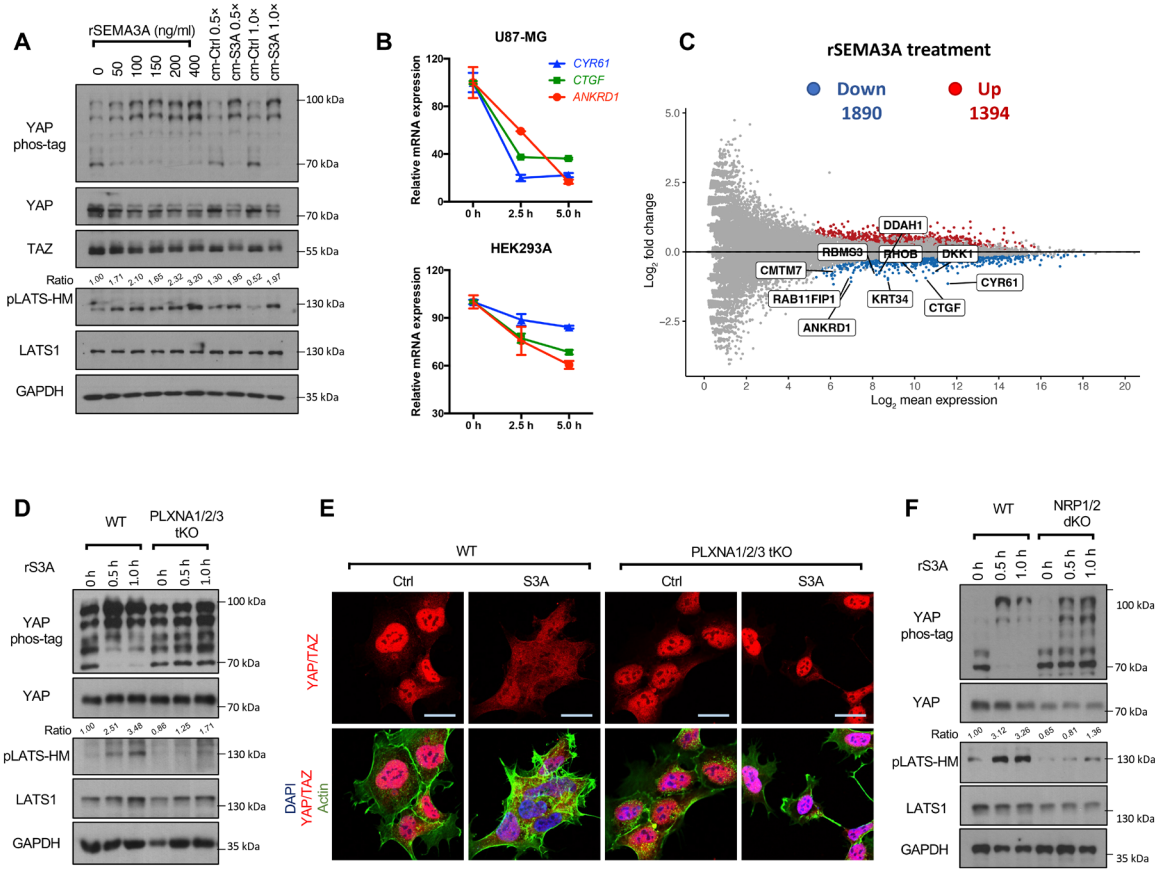

Fig. 1. SEMA3 induces YAP/TAZ phosphorylation and inactivation. (**A**) Sema3A activates the Hippo pathway. U87-MG cells were treated with human recombinant SEMA3A protein (rSEMA3A) or conditioned medium of cells expressing SEMA3A (cm-S3A). Phosphorylation of YAP and LATS was determined by phos-tag and phospho-specific antibodies, respectively. Slow migration on phos-tag gels indicates that proteins were hyperphosphorylated. 0.5× and 1.0× indicate that the conditioned medium was diluted twofold or undiluted, respectively. HM, hydrophobic motif; GAPDH, glyceraldehyde-3-phosphate dehydrogenase. (**B**) Quantitative real-time polymerase chain reaction (PCR) shows that SEMA3A inhibits expression of YAP/TAZ target genes (*CYR61*, *CTGF*, and *ANKRD1*) in U87-MG and HEK293A cells. (**C**) SEMA3A regulates Hippo signature genes. A volcano plot of the RNA-seq results showing that rSEMA3A protein decreased expression of YAP/TAZ signature genes in U87-MG cells. In total, 1890 genes were down-regulated, and 1394 genes were up-regulated. (**D**) Plexins are required for Hippo regulation by SEMA3A. Wild-type (WT) and PLXNA1/2/3 tKO HEK293A cells were treated with SEMA3A. Phosphorylation of YAP and LATS was determined as in (A). (**E**) SEMA3A induces YAP/TAZ cytoplasmic localization in a PLXNA-dependent manner. Immunofluorescence was performed to stain cells with YAP/TAZ antibody (red), 4′,6-diamidino-2-phenylindole (DAPI) (blue), and phalloidin (green for actin). Scale bars, 25 μm. (**F**) Deletion of NRP1/2 in HEK293A cells compromised SEMA3A-induced phosphorylation of YAP and LATS.

KO (dKO) cells (fig. S1, F and G) and subsequently found that deletion of NRP1/2 compromised SEMA3A-induced phosphorylation of LATS and YAP/TAZ (Fig. 1F), demonstrating that both PLXNA1/2/3 and NRP1/2 are required for SEMA3 to regulate the Hippo pathway.

Gene deletion or inactivation of type B and F of SEMA3 (SEMA3B and SEMA3F) has been frequently observed in human cancers, such as lung cancer, breast cancer, and renal carcinoma (*6*, *7*, *16*–*19*). Furthermore, previous studies have confirmed the tumor-suppressive role of SEMA3B and SEMA3F in lung cancer (*4*–*6*, *16*). We thus generated SEMA3B- and SEMA3F-conditioned medium to study their effects on YAP/TAZ activities and cell growth (fig. S2B). Similar to SEMA3A, both SEMA3B- and SEMA3F-conditioned media induced YAP/TAZ phosphorylation in multiple cell lines, including lung cancer cell lines NCI-H1792 and NCI-H1299 (Fig. 2A). These results further inspired us to characterize the connection between SEMA3 and the Hippo pathway in disease contexts.

SEMA3 controls transcriptome and inhibits cell growth via the Hippo pathway

We and others previously defined that YAP/TAZ phosphorylation is predominantly caused by the Hippo kinase cascade MST/MAP4K-LATS in mammalian cells in response to environmental signals (*10*, *20*). We examined whether the Hippo core kinase cascade is involved in YAP/TAZ regulation by SEMA3. Deletion of *LATS1/2* genes abolished SEMA3-induced phosphorylation and cytoplasmic translocation of YAP/TAZ in U87-MG and HEK293A cells (Fig. 2, B and C, and fig. S2C), as well as the lung adenocarcinoma cell line A549, for which LATS1/2 CRISPR-KO cell pools were also generated (fig. S2, D and E). Notably, YAP/TAZ phosphorylation in A549 cells was induced by SEMA3A treatment or high cell confluency but not by serum starvation (fig. S2E). Furthermore, deletion of the upstream Hippo kinases MST1/2 and MAP4K4/6/7 (*10*, *20*), two group protein kinases that activate LATS1/2 by directly phosphorylating their HM (*20*), also blocked YAP/TAZ phosphorylation caused by rSEMA3A treatment (fig. S2F). Consistently, rSEMA3A increased MST2 kinase activity toward LATS2 (fig. S2G) and promoted the interaction between MAP4K4 and LATS1 (fig. S2H). Together, these observations showed that SEMA3 acts via the Hippo kinase cascade to inactivate YAP/TAZ.

Because the major functional output of the Hippo signaling is YAP/TAZ-dependent transcription, quantitative real-time polymerase chain reaction (PCR) analysis was performed to confirm that the repression of YAP/TAZ target genes *ANKRD1* and *CTGF* by SEMA3A was compromised by the LATS1/2 deletion (Fig. 2D). To characterize whether the Hippo pathway is required for the global transcription regulation by SEMA3, we performed RNA-seq and principal components analysis (PCA) of SEMA3-treated WT and LATS1/2 dKO U87-MG cells. We found that LATS1/2 played an important role in the SEMA3-responsive transcriptome as a PCA reveals that the deletion of *LATS1/2* genes significantly reduce the transcriptomic responses to SEMA3A (Fig. 2E). We further performed a two-way analysis with DESeq2 to study the interaction between genotypes (LATS1/2 dKO versus WT) and treatments (SEMA3 versus control). The results showed that 36.4% (1195 of 3284) of the SEMA3-responsive genes (shown in Fig. 1C) were highly dependent on LATS1/2 (Fig. 2F). These LATS1/2-dependent SEMA3 target genes appear to be involved in cell cycle regulation, nuclear chromosome segregation, wound healing, and DNA replication (Fig. 2G), supporting the notion that the Hippo pathway mediates the well-known functional effects of SEMA3. It should be noted that our analysis was focused on the functional interaction between SEMA3 and LATS1/2. SEMA3 can also activate downstream targets other than LATS1/2. For instance, various RhoA effectors, other than Hippo pathway, will be inhibited by SEMA3. These effectors can play a crucial role in controlling cell functions (e.g., neuron axon guidance and cell migration) and gene transcription as reviewed recently (*21*). Furthermore, SEMA3 also regulates other non-LATS1/2 substrates of the Hippo kinases MST1/2 and MAP4K4/6/7. For instance, MAP4K4/6/7 can directly phosphorylate protein kinases including NDR (nuclear dbf2-related)1/2 (*22*) and transcription factors including SMAD and transcription factor 4 (*23*, *24*). These MAP4K substrates can play a crucial role in regulating global gene transcription.

The Hippo pathway mediates biological functions of SEMA3s in preventing carcinogenesis and angiogenesis

We observed that SEMA3 strongly inhibited the growth of HEK239A cells and U87 cells but did not affect the cell size (fig. S3, A and B). Deletion of LATS1/2 blocked the growth-inhibitory effect of SEMA3 in U87-MG and HEK293A cells (fig. S3B). The most characterized SEMA3s in tumor suppression are SEMA3B and SEMA3F, particularly in lung cancer (*6*, *7*, *16*–*19*). Our analyses of TCGA data also revealed that lung squamous cell carcinoma and lung adenocarcinoma (LUAD) showed substantial SEMA3B down-regulation compared with normal tissue (Fig. 3A). Neither SEMA3B nor SEMA3F gene is expressed in the NCI-H1299 lung cancer cells due to DNA methylation (*16*, *17*, *25*). To investigate the role of the Hippo pathway in tumor suppression by Semaphorin, we restored the expression of SEMA3B in both WT and LATS1/2 dKO NCI-H1299 cells using lentiviral transduction. The SEMA3B restoration increased YAP phosphorylation in the WT but not in the LATS1/2 dKO cells (Fig. 3B). Consistently, the SEMA3B reexpression led to growth inhibition only in the WT but not the LATS1/2 dKO NCI-H1299 cells (fig. S3C). Similar observations were made in another LUAD cell line NCI-H1792 (fig. S3D), which reportedly has minimal expression of SEMA3B (*17*).

To further examine the roles of this SEMA3-LATS1/2 signaling axis in lung cancer anchorage-independent growth and invasiveness, we performed a soft agar colony formation assay with the WT and the LATS1/2 dKO NCI-H1299 cells in which SEMA3B expression was restored. SEMA3B restoration substantially inhibited the growth of NCI-H1299 WT cells but not the LATS1/2 dKO cells (Fig. 3, C and D). Furthermore, SEMA3B reexpression significantly reduced the tumor growth of WT NCI-H1299 in xenografted mice in vivo, whereas tumor growth of the LATS1/2 dKO NCI-H1299 cells was largely insensitive SEMA3B reexpression (Fig. 3, E and F, and fig. S3E). These data support a key role of the Hippo pathway in mediating the tumor-suppressive activity of SEMA3 and suggest a therapeutic potential of SEMA3 gene restoration and YAP/TAZ inhibitors in lung cancer treatment.

Previous studies have indicated that Semaphorins are master regulators in endothelial homeostasis during development and disease development. Therefore, we speculate whether Hippo signaling mediates the function of Semaphorins in endothelial homeostasis. We thus generated LATS1/2 dKO human umbilical vein endothelial cell (HUVEC) pools and confirmed by LATS antibody Western blot (Fig. 3G). Conditioned SEMA3A medium or rSEMA3A proteins strongly induced phosphorylation of LATS and YAP in HUVECs

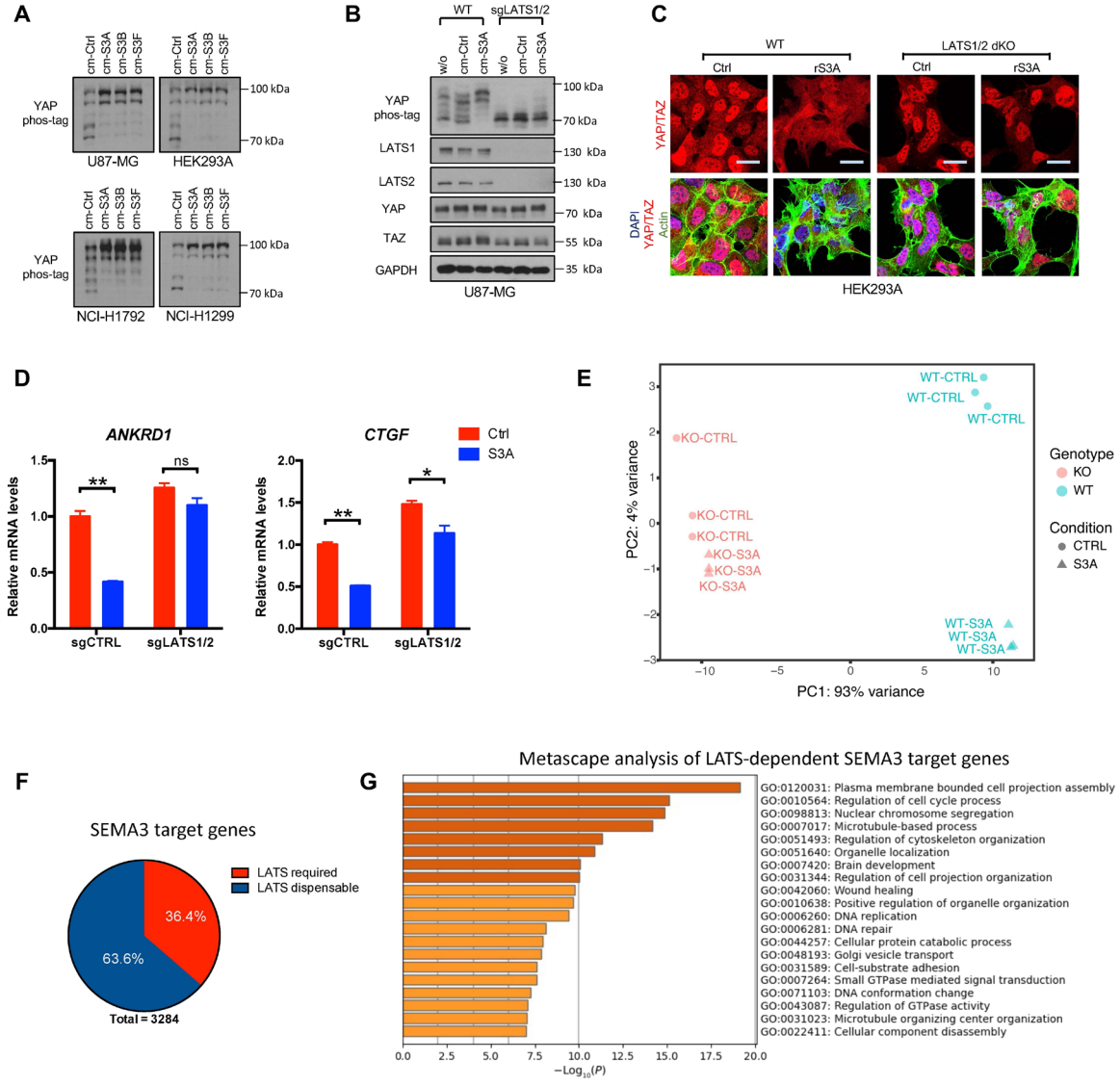

Fig. 2. SEMA3 inhibits cell growth via the Hippo pathway. (**A**) SEMA3B and SEMA3F induce YAP phosphorylation. Conditioned media (cm-S3A, cm-S3B, and cm-S3F) were used to treat U87-MG, HEK293A, NCI-H1792, and NCI-H1299 cells. YAP phosphorylation was detected by phos-tag gel. (**B**) LATS1/2 deletion blocks YAP phosphorylation by SEMA3A. U87-MG cells were infected with lentiviral CRISPR sgRNA (single guide RNA) constructs (sgLATS1/2), and deletions of LATS1 and LATS2 were detected by Western blots. Cells were treated with a control or SEMA3A-conditioned medium. w/o, without any conditioned medium added. (**C**) Deletion of LATS1/2 blocks SEMA3A-induced YAP cytoplasmic translocation in HEK293A cells. Scale bars, 25 μm. (**D**) *ANKRD1* and *CTGF* transcription repression by SEMA3A requires LATS. Quantitative real-time PCR analyses were performed with SEMA3A-treated WT and LATS1/2 dKO U87-MG cells. $*P < 0.05$; $**P < 0.01$; ns, not significant. (**E**) LATS1/2 deletion compromises SEMA3A-regulated transcriptome. Principal components analysis of the RNA-seq data of the WT and LATS1/2 KO U87-MG cells treated with or without rSEMA3A. PC, principal component. (**F**) A two-way (genotype and treatment) DESeq2 analysis of SEMA3-treated WT and LATS1/2 dKO cells showed that a substantial portion (36.4%) of genes regulated by the SEMA3 treatment is LATS1/2 dependent. (**G**) Hippo pathway mediates SEMA3 effects on biological functions such as cytoskeleton organization and wound healing. Metascape analysis of LATS-dependent SEMA3 target genes (F, red slice) was performed.

(Fig. 3G). As observed in other cell types, SEMA3 inhibits the growth of HUVECs in a LATS1/2-dependent manner (fig. S3F). SEMA3 restricts angiogenesis via its roles in endothelial cell migration and morphogenesis (*1*, *2*). We observed that SEMA3 also required LATS1/2 to inhibit tube formation (Fig. 3H), which indicates the capability of endothelial cells to form blood vessels (*26*). The LATS1/2 dKO HUVECs not only are resistant to SEMA3 inhibition but also form more stable and structured tubes in this assay. We further performed an in vivo plug assay to evaluate the SEMA3 effects on angiogenesis in a mouse model (*27*). Histological analyses of blood vessels and immunoflurosence of $CD31^+$ endothelial cells in the plugs also demonstrated that SEMA3 overexpression required LATS1/2 to repress blood vessel formation in vivo (Fig. 3, I to K). Furthermore, transwell migration of HUVECs was suppressed by conditioned medium from SEMA3B-reexpressing NCI-H1299 cells but not that from control cells. This inhibitory activity of SEMA3B was also abolished by LATS1/2 deletion (Fig. 3L). The above observations imply that, in the tumor microenvironment, cancer cells lost the ability to

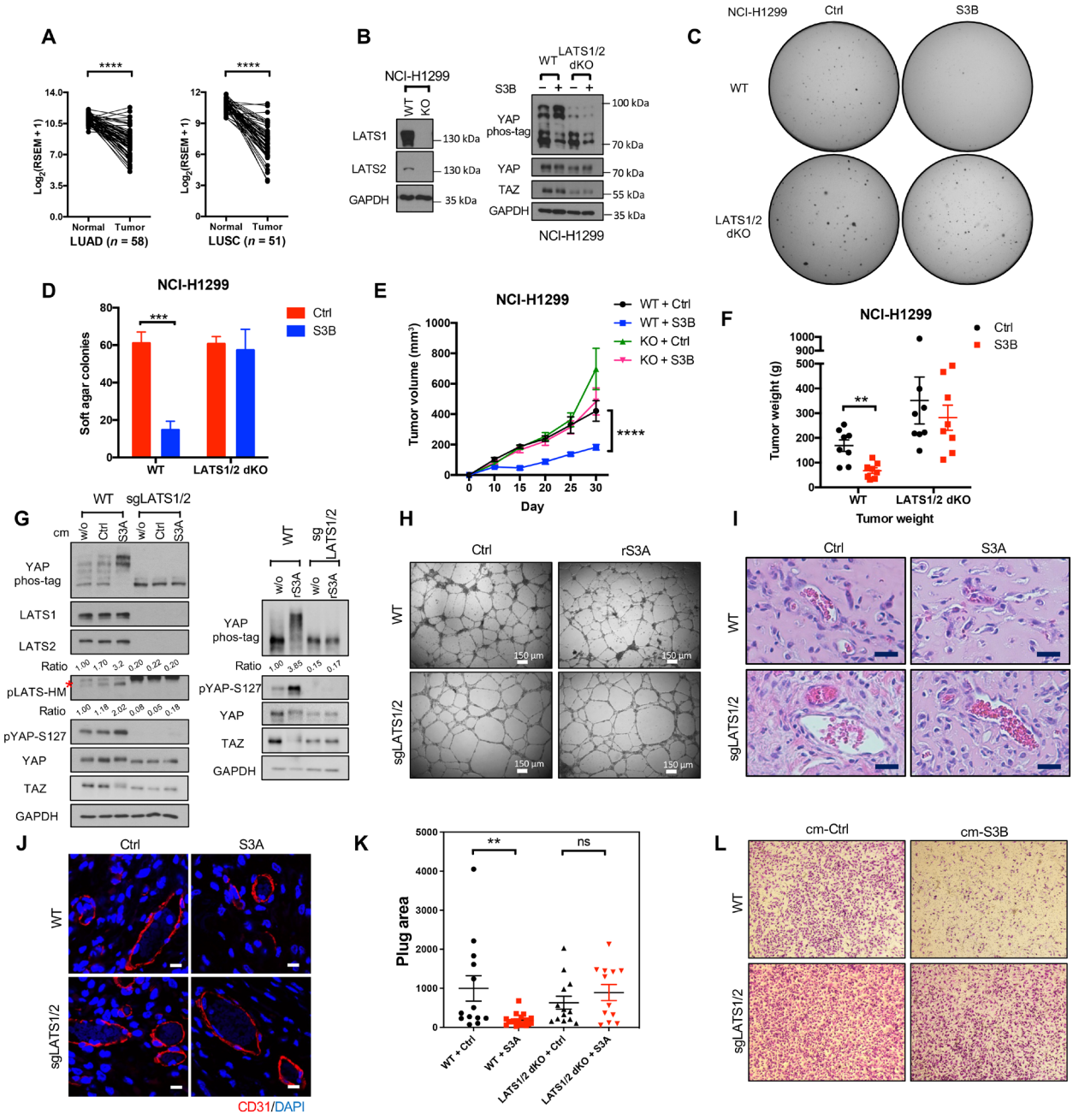

Fig. 3. The Hippo pathway mediates the biological functions of SEMA3s. (**A**) SEMA3B is down-regulated in lung cancers. ****$P < 0.0001$, Wilcoxon matched-pairs signed-rank test. LUSC, lung squamous cell carcinoma. RSEM, RNA-seq by expectation-maximization. (**B**) Deletion of LATS1/2 in NCI-H1299 cells block SEMA3B-induced YAP/TAZ phosphorylation. The left panel shows the KO efficiency of LATS1 and LATS2, while the right panel shows YAP phosphorylation by SEMA3B. (**C**) Suppression of anchorage-independent colony formation in NCI-H1299 cells by SEMA3B requires LATS1/2. A representative image was shown for triplicates in each group. Notably, LATS1/2 dKO formed larger colonies, and SEMA3B still reduced colony size in LATS1/2 dKO cells, suggesting that SEMA3B may attenuate colony growth by additional mechanisms. (**D**) Quantification of (C). ***$P < 0.001$, two-tailed t test, $n = 3$; $n = 3$. (**E**) Inhibition of NCI-H1299 xenograft volume by SEMA3B requires LATS1/2. ****$P < 0.0001$, two-way analysis of variance (ANOVA) test, $n = 8$. The results shown here are representative of two independent animal trials. (**F**) Measurement of tumor weights. **$P < 0.01$, two-tailed t test, $n = 8$. (**G**) Deletion of LATS1/2 in HUVECs blocks YAP phosphorylation induced by SEMA3A-conditioned medium. (**H**) Recombinant SEMA3A proteins inhibit tube formation of WT but not LATS1/2 dKO HUVECs. (**I**) Hematoxylin and eosin staining of an in vivo plug assay using WT and LATS1/2 dKO HUVECs inoculated into nonobese diabetic/severe combined immunodeficient mice. SEMA3A gene expression was introduced to the cells by lentiviral transduction. Mature blood vessels with blood are shown in the representative images. Scale bars, 50 μm. (**J**) CD31 staining of endothelial cells in the plugs. Scale bars, 20 μm. (**K**) Quantification and statistical analysis of (J). **$P < 0.01$, S3A versus Ctrl, Student's t test was performed. (**L**) Conditioned medium from SEMA3B-restored NCI-H1299 cells, but not from the control cells, inhibits transwell migration of HUVECs in a LATS1/2-dependent manner.

suppress angiogenesis due to SEMA3 deficiency, while normal lung cells secrete SEMA3 to inhibit angiogenesis.

p190RhoGAP mediates YAP/TAZ inhibition by SEMA3 and PLXNA

We next investigated the mechanisms by which PLXNA1/2/3 and NRP1/2 mediate SEMA3A signals to the Hippo kinase cascade. PLXNAs were recently reported as GTPase activating proteins (GAPs) for Ras-related protein 1 (RAP1) and RAP2 (*28*, *29*). One possible model is that SEMA3 acts through PLXNA to inactivate RAP1 and/or RAP2 to induce YAP/TAZ phosphorylation. However, RAP2 is known to induce YAP/TAZ phosphorylation (*11*), inconsistent with the above model. Deletion of RAP2 reduced YAP phosphorylation, although the response to SEMA3 was also compromised (fig. S3F). Furthermore, expression of a constitutively active RAP1 had minimal effect on SEMA3-induced YAP/TAZ phosphorylation (fig. S3G). On the basis of these results, RAP1 and RAP2 are unlikely to be the key downstream effectors responsible for YAP/TAZ inhibition by SEM3A.

To identify the downstream mediators of PLXNA, we used a TurboID approach to label PLXNA1 proximal proteins (*30*). We fused the TurboID biotin ligase to the C terminus of PLXNA1 and expressed the PLXNA1-TurboID fusion proteins, as well as corresponding controls, in U87-MG cells. We then labeled the potential interacting proteins with biotin after rSEMA3A treatment as illustrated in Fig. 4A. Tandem mass tag (TMT) labeling combined with liquid chromatography–mass spectrometry (LC-MS) was used to analyze the proteins recruited to PLXNA1 upon rSEMA3A treatment. PLXNA1, even in the absence of rSEMA3A, already interacted with quite a few Hippo components (Merlin/NF2, PTPN14, SCRIB, SCRIB, ITGB2, MAP4K4, MAP4K5, and MINK1/MAP4K6) and many RhoGAP proteins (ARHGAP1/22/31/35/39) (Fig. 4B, top). However, only the interaction between ARHGAP35/p190RhoGAP-A with PLXNA1 was significantly increased by rSEMA3A treatment (Fig. 4B, bottom, and tables S1 to S3). We further confirmed this dynamic interaction between PLXNA and ARHGAP35 by coimmunoprecipitation (Fig. 4C).

To test whether ARHGAP35 and its closest homolog ARHGAP5/p190RhoGAP-B are involved in the Hippo pathway regulation by SEMA3, we overexpressed ARHGAP35 and ARHGAP5 in HEK293A cells and found that both ARHGAP35 and ARHGAP5 could induce YAP phosphorylation (fig. S4A). Both the canonical Hippo kinases MST1/2 and noncanonical Hippo kinases MAP4K4/6/7 were involved in the YAP phosphorylation induced by ARHGAP5/35 (fig. S4B). Deletion of both ARHGAP5 and ARHGAP35 in two different CRISPR-KO clones consistently blunted the SEMA3A-induced phosphorylation and cytoplasmic translocation of YAP/TAZ (Fig. 4, D and E, and fig. S4C). These data show that the two p190RhoGAPs are required for the Hippo regulation by SEMA3.

The pseudo-GTPase domain of ARHGAP35 interacts with PLXNA1 and facilitates ARHGAP35 activation by PLXNA1-recruited RND GTPases

To understand the mechanisms by which PLXNA interacts with ARHGAP35 and activates the Hippo pathway, we analyzed the structural domains of ARHGAP35 (Fig. 5A). These include an N-terminal Ras-like pseudo-GTPase [constitutive guanosine 5′-triphosphate (GTP) binding], four FF domains, two middle pseudo-GTPase domains (nucleotide-binding deficient), a lipid-binding domain, and a C-terminal GAP domain (known to target RhoA or Rac1 GTPase) (*31*). RhoA GTPase has been implicated to regulate the Hippo-YAP signaling. However, a previous study shows that inhibition of Rho GTPases by ARHGAP5/35 is insufficient to inactivate YAP (*32*). To test whether RhoA inhibition can result in YAP phosphorylation through the Hippo kinase cascade, we applied three different approaches—RhoA inhibitor C3 treatment, dominant-negative RhoA overexpression, and RhoGDI overexpression—to inhibit RhoA. All the three different approaches induced YAP phosphorylation in a LATS1/2-dependent manner (fig. S4, D to F). Both canonical Hippo kinases MST1/2 and noncanonical Hippo kinases MAP4K4/6/7 are involved in this effect of Rho inhibition on YAP phosphorylation. Rescuing ARHGAP5/35 dKO HEK293A cells with an ARHGAP35 without the RhoGAP domain (dGAP) (fig. S4G) could not restore SEMA3A-induced YAP phosphorylation in contrast to the rescue by the full-length ARHGAP35 (WT) (Fig. 5B). These results together connect PLXNA1 to ARHGAP35 and then to RhoA GTPase and the Hippo kinase cascade.

The N-terminal GTPase domain and its nucleotide-binding were also important for ARHGAP35 to mediate SEMA3A-induced YAP phosphorylation, as ARHGAP35 with the deletion of N-terminal GTPase (dGAP) or the mutation of nucleotide-binding residue (S36N) could not fully rescue SEMA3A-induced phosphorylation of YAP and LATS (Fig. 5B). Furthermore, a constitutively active N-terminal GTPase mutant (G29V) even slightly enhanced YAP phosphorylation. We speculate that the N-GTPase domain likely creates an interaction interface between ARHGAP35 and PLXNA1 as implicated from a previous structural biology study (*31*), and this interaction is essential for PLXNA1 to activate ARHGAP35. Therefore, we performed a coimmunoprecipitation between PLXNA1 and ARHGAP35 with deletion of various domains (fig. S4G). We found that the N-GTPase domain was indeed required for interaction with PLXNA1 (Fig. 5C). On the other hand, deletion of any intracellular domains in PLXNA1 prevented its interaction with ARHGAP35 (Fig. 5D), suggesting that the overall structural integrity or the configuration of PLXNA1 is essential for the ARHGAP35 interaction.

To gain more insights into the mechanism by which PLXNA1 activates p190RhoGAP upon SEMA3 treatment, we searched other related p190RhoGAP upstream regulators and noticed that small GTPases RND1 and RND3 have been reported to activate ARHGAP35 and interact with both PLXNA1 and p190RhoGAP (*33*–*36*). To test the roles of RND1/3 in the SEMA3-Hippo signaling, we expressed the mouse PLXNA1 mutant that is deficient in RND binding (LVP1598-1600GGA) (*35*, *36*) and found that only the WT PLXNA1, but not the GGA mutant, could rescue the SEMA3 responses in PLXNA1/2/3 tKO cells (Fig. 5E). We subsequently investigated the effects of RND on YAP/TAZ phosphorylation. Ectopic overexpression of RND GTPases triggered YAP/TAZ phosphorylation in a dose-dependent manner (Fig. 5F and fig. S5A). Deletion of RND1 and RND3 (fig. S5B), the two RND GTPases that are located at the plasma membrane and respond to SEMA3 (*34*), nearly abolished SEMA3A-induced YAP/TAZ phosphorylation (Fig. 5G). However, in contrast to the WT, RND mutants deficient in ARHGAP35 binding (RND1-T45A and RND3-T55A) lost the ability to induce YAP phosphorylation (fig. S5C). SEMA3 could rapidly induce the interaction between RND1 and ARHGAP35 in a time- and dose-dependent manner (Fig. 5H and fig. S5D), and this enhancement required both the receptor binding domain (RBD) and the GAP domain of PLXNA1 (fig. S5E). Together, these data suggest that RND GTPases are key mediators acting between PLXNA and ARHGAP35 to relay SEMA3 signals to the Hippo pathway.

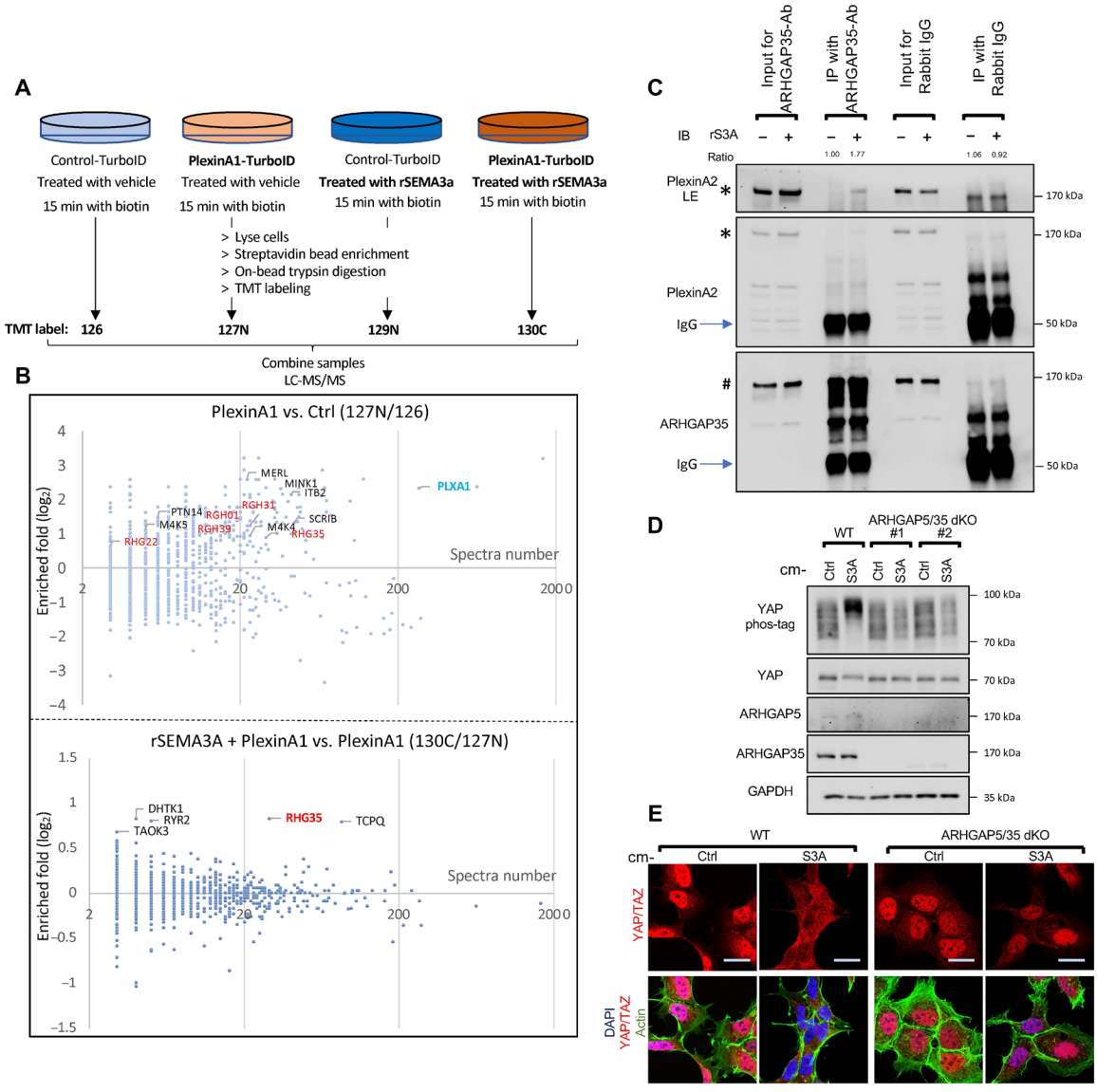

Fig. 4. p190RhoGAP mediates YAP/TAZ inhibition by SEMA3 and PLXNA. (**A**) A flow chart illustrating the TurboID-Mass Spectrometry that was used to identify proteins whose interactions with PlexinA are affected by rSEMA3A treatment. (**B**) A graph showing proteins that inherently or dynamic interacts with PlexinA1 before and after SEMA3 treatment. Notably, many RhoGAPs (RHGs) interact with PlexinA1, but only p190RhoGAP-A (ARHGAP35, RHG35) increases its interaction with PlexinA1 upon rSEMA3A treatment. (**C**) A coimmunoprecipitation of endogenous ARHGAP35 and PlexinA2 using an ARHGAP35 antibody. The star (*) indicates PlexinA2, and # indicates ARHGAP35. IB, immunoblot; IP, immunoprecipitation; IgG, immunoglobulin G. (**D**) Deletion of ARHGAP5/35 in HEK293A cells blocks rSEMA3A-induced phosphorylation and (**E**) cytoplasmic translocation of YAP. Scale bars, 25 μm.

Loss of function of RND1/3 and ARHGAP5/35 compromises SEMA3-induced growth inhibition of cancer cells

Both RND1 and ARHGAP35 have been implicated as tumor suppressor genes, and hotspot and truncated mutations of these genes are observed in human cancers (*32*, *37*). Knockdown of RND1/3 or ARHGAP5/35 by RNA interference (RNAi) (fig. S6, A and B) substantially compromised SEMA3-induced YAP phosphorylation (fig. S6C) and growth inhibition in non–small cell lung cancer NCI-H1792 cells (Fig. 6A). We next asked whether the cancer-associated hotspot mutations affect their function in the Hippo pathway regulation by SEMA3. RND1-G70R is a reoccurring mutant in breast cancer (*37*). We found that, unlike the WT RND1, overexpression of the RND1-G70R mutant was unable to induce YAP phosphorylation or to interact with ARHGAP35 (Fig. 6B and fig. S6D). Next, we examined whether the hotspot mutations in RND1, RND3, or ARHGAP35 affect their abilities in mediating SEMA3 signaling to YAP phosphorylation and cell growth inhibition. The tumor-derived mutants of RND1/3 and ARHGAP35 were expressed in RND1/3 dKO and ARHGAP5/35 dKO cells, respectively (fig. S6, E and F). Several mutations—including E98D and M185V of RND1, S95L of RND3, and V1317M of ARHGAP35—were compromised in their ability to restore the YAP phosphorylation (Fig. 6C) and growth inhibition (Fig. 6D) in response to SEMA3 treatment. On the basis of the TCGA PanCancer Atlas studies, a substantial number (164 among

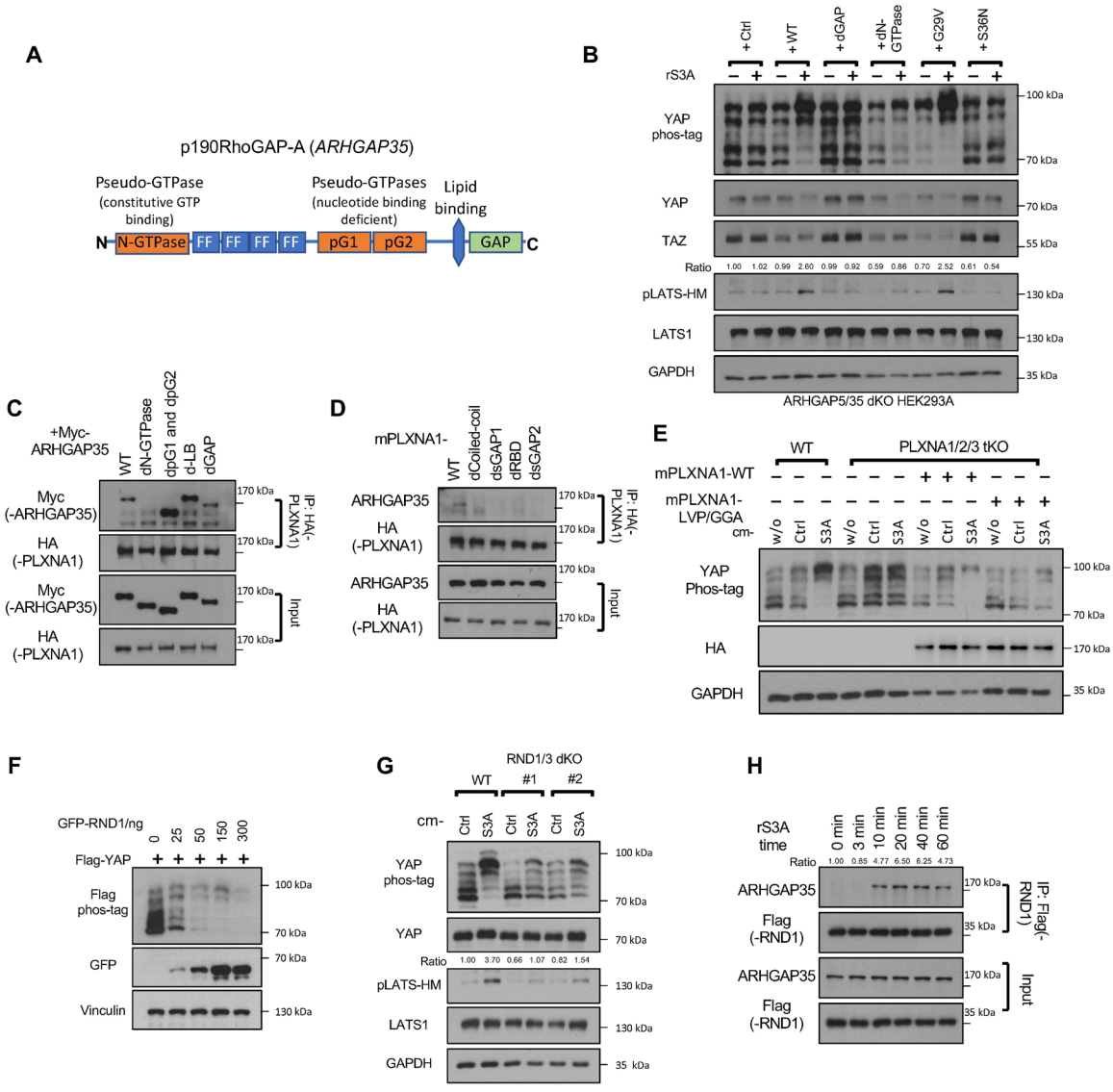

Fig. 5. The pseudo-GTPase domain of p190RhoGAP creates an interactive interface for PLXNA1 binding and facilitates p190RhoGAP activation by RND GTPases. (**A**) Schematic illustration of p190RhoGAP-A functional domains. There are an N-terminal pseudo-GTPase domain (constitutive GTP-binding), four FF domains, two pseudo-GTPase domains (pG1 and pG2, deficient in nucleotide binding), a lipid-binding (LB) domain, and a C-terminal RhoGAP domain. (**B**) The N-GTPase domain and the C-terminal RhoGAP domain are involved in SEMA3-induced YAP phosphorylation. Reexpression of WT, RhoGAP-deleted (dGAP), N terminal GTPase-deleted (dN-GTPase), active GTPase (G29V), and inactive GTPase (S36N) mutant of ARHGAP35 was done in ARHGAP5/35 dKO cells. (**C**) PLXNA interacts with ARHGAP35 via the N-GTPase domain. Hemagglutinin (HA)–PLXNA1 and Myc-ARHGAP35 deletion mutants were co-transfected into HEK293A cells. HA-PLXNA1 was immunoprecipitated, and coprecipitated Myc-ARHGAP35 mutants were detected by Western blot. Deletion of the N-GTPase domain—but not pG1 and pG2, LB, and RhoGAP domains—of ARHGAP35 affects the PLXNA1 interaction. (**D**) Deletion of the coiled-coil domain, segmented GAP domains (sGAP1 and sGAP2), and RBDs of PLXNA1 abolished interaction between ARHGAP35 and PLXNA1. HA-tagged PLXNA1 plasmids encoding deletion mutants were transfected into HEK293A cells that were then treated with SEMA3. Western blot with HA and ARHGAP35 antibodies was used to analyze the coimmunoprecipitants. (**E**) RND binding to PLXNA1 is required for SEMA3-induced YAP phosphorylation. WT and RND-binding deficient (LVP → GGA) mutant mouse PLXNA1 was reexpressed in PLXNA1/2/3 tKO cells, which were treated with SEMA3A. (**F**) RND1 induces YAP phosphorylation. Green fluorescent protein (GFP)–RND1 was transfected in HEK293A cells. GFP-RND1 expression and YAP phosphorylation were determined. (**G**) Deletion of RND1/3 blocks SEMA3A-induced phosphorylation of YAP and LATS in HEK293A cells. (**H**) Interaction between RND and ARHGAP35 is enhanced by SEMA3 in a time-dependent manner. Flag-RND1–transfected HEK293A cells were treated with rSEMA3A and harvested at the indicated time. Coimmunoprecipitation was performed to analyze interaction between RND1 and ARHGAP35.

443 in total) of ARHGAP35 mutations in cancers are truncating mutations, which result in loss of the C-terminal RhoGAP domain and are predicted to be inactive to regulate the Hippo pathway based on our data (Fig. 5B). These results further support the role of RND1/3 and ARHGAP5/35 in SEMA3 signaling and the tumor suppressor function of SEMA3 through Hippo pathway activation.

Oscillatory shear stress blocks SEMA3A-induced YAP/TAZ inactivation

Mechanical cues—such as cell-cell contact, matrix stiffness, and flow shear—can regulate Hippo signaling (*11*, *38*). PLXND1 and PLXNB1/2 were reported to respond to mechanical cues to modulate cell behaviors (*39*–*41*). For example, laminar and oscillatory shear can

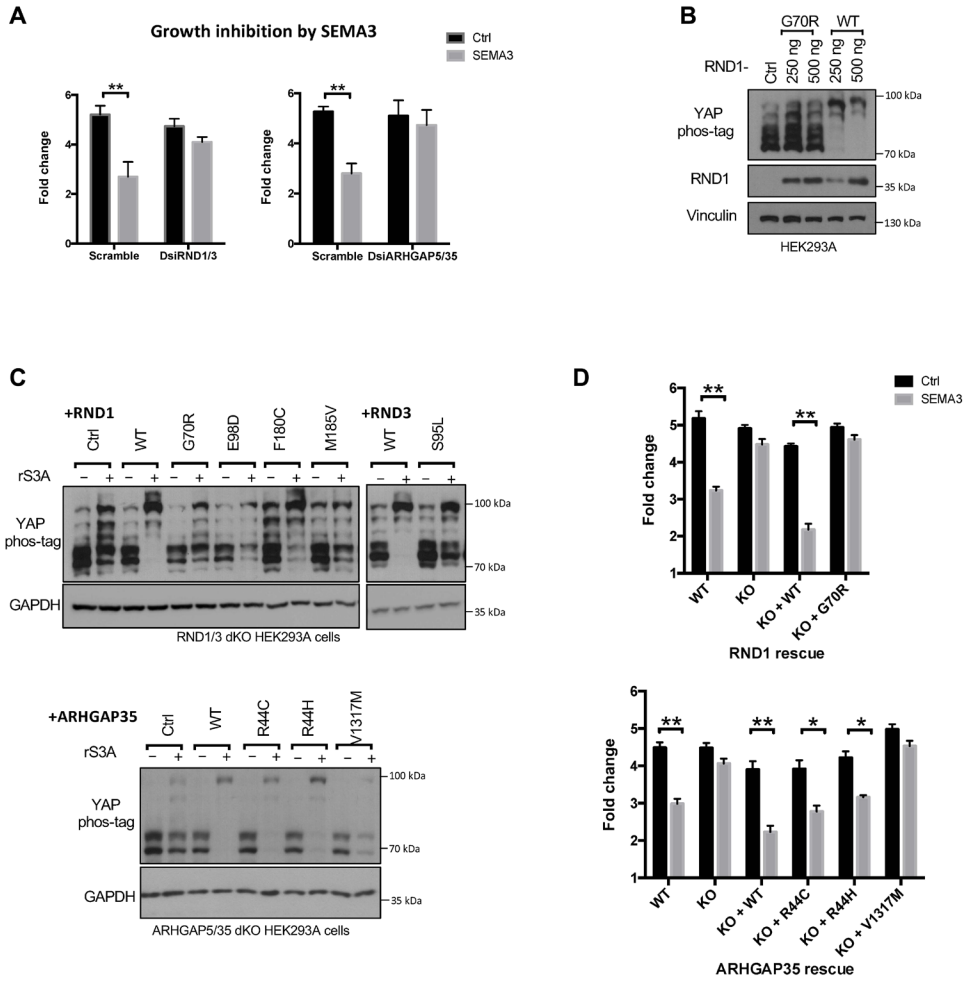

Fig. 6. Loss of function of RND1/3 and ARHGAP5/35 compromises SEMA3-induced growth inhibition of cancer cells. (**A**) Knockdown of RND1/3 and ARHGAP5/35 compromised SEMA3 inhibition of NCI-H1792 cells. Duplex RNAi oligos were used to knock down the target genes. The cells were treated with SEMA3 3 days after transfection of RNAi. Two-tailed Student's *t* test was performed. $^{**}P < 0.01$. (**B**) RND1 G70R, a cancer-associated mutation, is unable to induce YAP phosphorylation. RND1 plasmids (250 or 500 ng) were transfected into cells growing on six-well plates. (**C**) Cancer-associated mutants of RND and ARHGAP35 are defective in mediating YAP regulation by SEMA3A. Various mutants of RND1/3 and ARHGAP35 were expressed in RND1/3 KO cells and ARHGAP35 dKO cells, respectively. Cells were then treated with SEMA3 recombinant proteins. (**D**) Cancer-associated mutants of RND and ARHGAP35 are defective in mediating cell growth regulation by SEMA3A. Cell growth after 2-day SEMA3A-conditioned medium treatment was analyzed. Two-tailed Student's *t* test was performed. $^{*}P < 0.05$ and $^{**}P < 0.01$.

regulate PLXND1 configuration to influence cellular mechanoresponses during atherosclerosis. During development, cell-cell contact may also act through PLXNB to control YAP/TAZ subcellular location, but the exact effects of plexins on YAP activity are not entirely consistent among different studies (*39*–*41*). We observed that overexpression of PLXNA1 or PLXND1 did not counteract YAP phosphorylation by high cell density, whereas expression of the positive control lysophosphatidic acid receptor LPAR1 decreased YAP phosphorylation (Fig. 7A). PLXNA1 overexpression slightly increases YAP phosphorylation. Considering the key roles of PLXNA in endothelial homeostasis (*1*), we examined whether shear stress may affect cellular responses to PLXNA ligand SEMA3. We found that atherosclerosis-mimicking oscillatory shear decreased the phosphorylation of LATS1/2 and YAP and promoted YAP/TAZ nuclear localization (fig. S7, A to C). Notably, oscillatory flow shear stress abolished YAP/TAZ regulation by SEMA3s (Fig. 7, B and C, and fig. S7D). This was further confirmed by our quantitative real-time PCR of YAP target genes (fig. S7E). All these data indicate that, under atherosclerotic conditions, endothelial cells may encounter compromised YAP/TAZ regulation by physiological SEMA3s, thus contributing to the disease progression.

To understand how oscillatory shear blocks the activity of SEMA3A in Hippo pathway regulation, we determined the activity of RhoA and Rac1 under SEMA3 treatment and/or oscillatory shear. RhoA, but not Rac1, was inhibited and activated by SEMA3A and oscillatory shear, respectively (Fig. 7D). Notably, oscillatory shear nearly abolished the inhibitory effect of SEMA3A on RhoA. We further examined the interaction between PLXNA1 and its downstream interactors ARHGAP35 and RND1 in response to oscillary shear (Fig. 7E). Oscillatory shear had little effect on the interaction between RND1 and ARHGAP35 or PLXNA1. These results imply that oscillary shear uses mechanisms different from SEMA3 in Hippo regulation, and components downstream of ARHGAP35 may account for the effect of oscillatory shear on Hippo signaling. Oscillatory

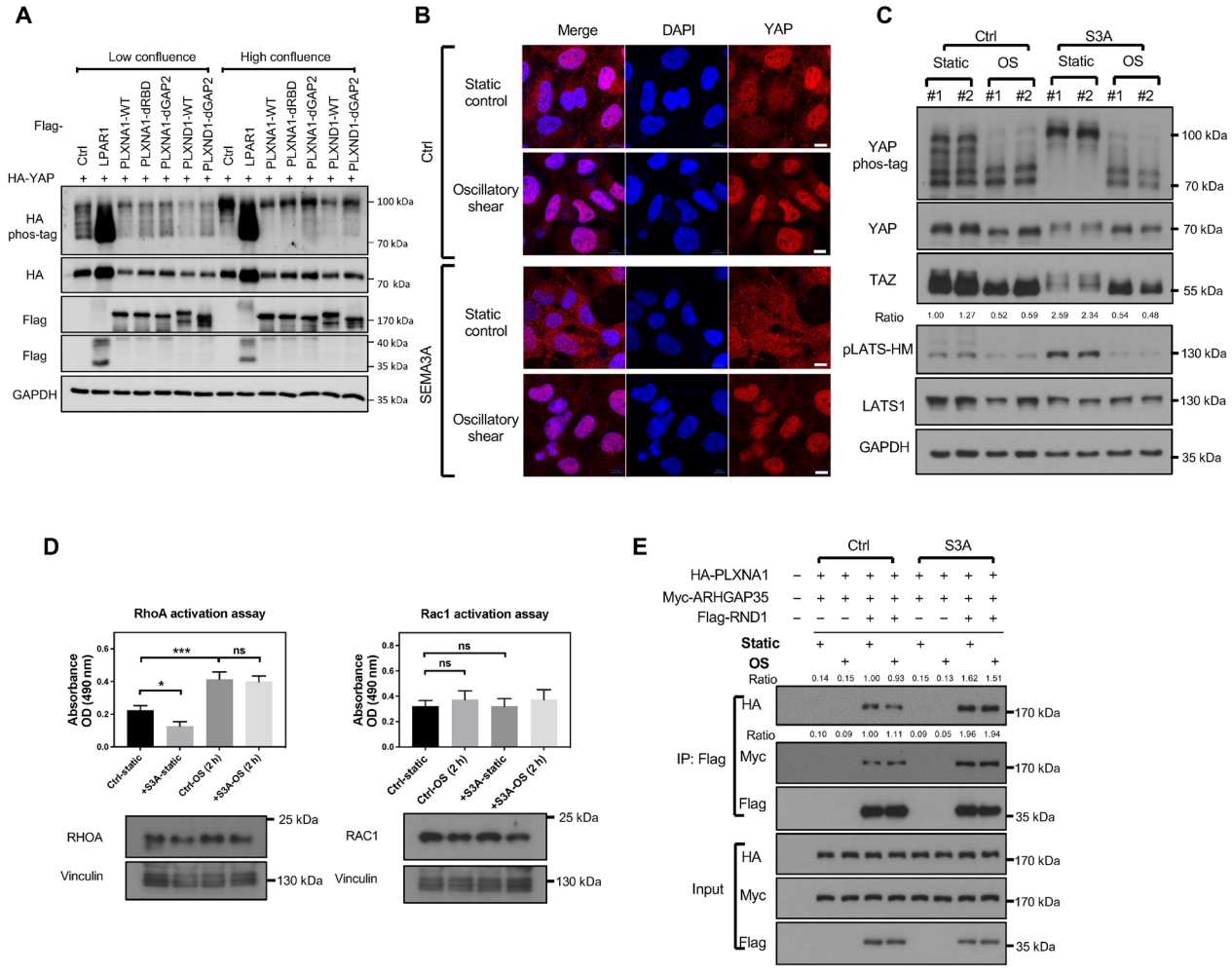

Fig. 7. Oscillatory shear stress blocks SEMA3A-induced YAP/TAZ dephosphorylation and cytoplasmic localization. (**A**) PLXNA1 overexpression modestly increases YAP phosphorylation. N-terminal tagged PLXNA1, PLXND1, and their mutant forms are cotransfected with HA-tagged YAP into HEK293A cells, which are seeded at the low or high confluence as previously described (*20*). LPAR1 denotes the lysophosphatidic acid receptor. (**B**) Oscillatory shear stress blocks SEMA3A-induced YAP/TAZ cytoplasmic localization. HEK293A cells were treated with oscillatory shear stress for 2 hours in the conditioned medium of cells expressing SEMA3A or control vector. Immunofluorescence was performed to stain cells with YAP/TAZ antibody (red) and DAPI (blue). (**C**) Oscillatory shear (OS) stress blocks SEMA3A-induced Hippo pathway activation. Phosphorylation of YAP and LATS was determined by phos-tag and phospho-specific antibodies, respectively. (**D**) RhoA, not Rac1, is activated by oscillatory shear, which also blocks the deactivation of RhoA induced by SEMA3A. After indicated treatments, these cells were lysed and incubated with RhoA-GTP or Rac1-GTP–binding strips. The active GTP-bound Rho protein was recognized by specifically primary antibodies and horseradish peroxidase (HRP)–linked secondary antibody. Signal was measured using a microplate spectrophotometer. The bottom panel was the total protein level of RhoA/Rac1 in cell lysates. OD, optical density. (**E**) Oscillatory shear stress does not affect interaction among RND1, p190RhoGAPs, and PLXNA1. HA-PLXNA1, Myc-ARHGAP35, and Flag-RND1 were cotransfected into HEK293A cells. HEK293A cells were treated with oscillatory shear stress for 2 hours in the conditioned medium of cells expressing SEMA3A or control vector. Flag-RND1 was immunoprecipitated, and coprecipitated Myc-ARHGAP35 and HA-PLXNA1 were detected by Western blot.

shear activated RhoA GTPase (Fig. 7D) (*42*), which is well known to regulate the Hippo pathway. We posit that RhoA activation by oscillatory shear antagonizes the effect of SEMA3s on the Hippo pathway.

DISCUSSION

SEMA3s have been regarded as fate-determining molecules in many biological processes, including neural axon guidance, cell growth control, migration, invasion, and angiogenesis (*1*); however, the downstream effectors of SEMA3/PLXNA in these processes have not yet been systematically defined.

In our study, we performed several functional genomics and proteomics studies to uncover that the Hippo pathway acts as a key mediator for the function of SEMA3 in cell growth inhibition and tumor suppression. Numerous genetic studies have established a key positive role of YAP/TAZ in angiogenesis (*43*), while one of the best established Semaphorin functions is anti-angiogenesis (*1*). Our study suggests that inhibition of YAP/TAZ may represent one mechanism for Semaphorins to control angiogenesis. Moreover, the SEMA3A-induced transcriptome, particularly the transcription repression, is highly dependent on the Hippo pathway. Mechanistically, the SEMA3 receptor PLXNA serves as a docking site for RND GTPases and

p190RhoGAPs (ARHGAP5/35) through its RBD and the segmented GAP domains, respectively (Fig. 5). Notably, the function of pseudo-GTPase domains is emerging only very recently through structural analyses of ARHGAP5/35 proteins, which is believed to provide an interactive interface for upstream regulators (*31*, *44*). In this study, we found that the pseudo-GTPase domain of ARHGAP5/35 directly interacts with the segmented GAP domains of PLXNA. PLXNA thus promotes ARHGAP5/35 to interact with RND upon SEMA3 binding, resulting in RhoA inhibition. When RhoA is inactivated, the Hippo kinase cascade is activated by striatin-interacting phosphatase and kinase (STRIPAK) complexes and/or the actin cytoskeleton (fig. S7F) (*20*). Our study thus defines the PLXNA-RND-p190RhoGAP signaling axis as a key link connecting the morphogen SEMA3 to the core Hippo kinases and provides the first example of the p190RhoGAP pseudo-GTPase domains mediating intracellular signal transduction to control cancer cell growth. In addition, the RND-p190RhoGAP-Hippo signaling may work in parallel to RND-RAP1-p120RasGAP to mediate the growth inhibitory effects of Semaphorins as previously reported (*37*).

Future studies are needed to comprehensively characterize how the SEMA3-Hippo signaling is dysregulated in disease microenvironments. Many components of this pathway are inactivated by genetic mutations as we illustrated (Fig. 6). Furthermore, mechanical cues can also modulate the sensitivities of this signaling (Fig. 7). More studies are needed to understand how disease cues contribute to pathogenesis by inactivating the SEMA3-Hippo signaling in contexts including cell migration, angiogenesis, cancer metastasis, and fibrosis, where both SEMA3 and YAP/TAZ are known to play important roles. As both Semaphorins and YAP/TAZ inhibitors are now regarded as new therapeutic agents, our study suggests potential novel therapies for diseases associated with aberrant SEMA3-Hippo signaling.

MATERIALS AND METHODS

Plasmids

The plasmids containing human SEMA3B and SEMA3F or ARHGAP5/35 protein coding sequences were purchased from transOMIC Technologies. Then, the coding sequences were subcloned into expression plasmids. The green fluorescent protein–tagged RND1/2/3 plasmids were gifts from C. Der. (Addgene, #23227, #23228, and #23229).

CRISPR-Cas9 system was used to delete genes in HEK293A, U87-MG, and A549 cells. The plasmids px459 v2 and lentiCRISPR v2 were provided by F. Zhang (Addgene, #62988 and #52961). The single guide RNA sequences targeting individual genes were shown in supplementary figures, or described previously (*11*), or as follows:

ARHGAP5 (#1: ACTATACTGATGGTATAGGA; #2: ATACTGATGGTATAGGATGG) and ARHGAP35 (#1: CACCACACTGATGTTGTAGG; #2: GTCACTGGTGCTGAGGACGG). The Duplex RNAi for RND1/3 or ARHGAP5/35 and control RNAi Duplex were purchased from IDT DNA Technology and transfected into the cells by Lipofectmine RNAiMAX (Thermo Fisher Scientific).

Cell culture

HEK293A were described previously (*11*, *20*). U87-MG cells were purchased from the American Type Culture Collection. U373-MG, A549, NCI-H1299, and NCI-H1792 cells were gifts from D. Cheresh at University of California, San Diego. Conditioned medium for SEMA3 was prepared from HEK293A cells stably expressing SEMA3. For SEMA3 treatment, cuture medium was changed 1 hour before the recombinant proteins, or conditioned medium was added to eliminate the effects of the basal level of SEMA3 secretion from the cells.

Staining and microscopy

For immunofluorescence, cells were fixed in 4% formaldehyde/phosphate-buffered saline (PBS) for 10 min and then were treated with 0.1% Triton X-100 for 15 min. After blocking, the cells were stained with corresponding antibodies. Most images were captured with a Nikon Eclipse Ti confocal microscope and then were exported from NIS elements imaging software. The quantification of plug area was performed by ImageJ software.

Animal studies

Eight- to 9-week-old female nude mice were purchased from the Jackson Laboratory. The mice were hosted in a specific pathogen–free room under standard 12-hour light/12-hour dark cycle, fed with standard rodent chow and water ad libitum, and randomized before experiments. The sample size choice was not predetermined for each experiment. The investigators are blinded to group allocations during data collection and analyses. All the procedures followed the National Institutes of Health *Guidelines for the Care and Use of Laboratory Animals*, and the Institutional Animal Care and Use Committee at the University of California, San Diego approved the experiments. For subcutaneous tumor growth, the maximum single tumor cannot exceed 2 cm in diameter in mice, and no experiments in the study generated tumor burden over this limit. The plug assay was performed on the basis of previously published protocols (*27*, *45*). Briefly, 2×10^6 WT and LATS1/2 dKO HUVECs with or without SEMA3A expression were embedded into growth factor–reduced Matrigel and then inoculated into nonobese diabetic/severe combined immunodeficient mice (JAX) via subcutaneous injections. The plugs were recovered 14 days after the inoculation.

Quantitative real-time PCR

Total RNAs were extracted with a kit from QIAGEN. Reverse transcription was performed with iScript from Bio-Rad. The real-time PCR was performed with the Applied Biosystems 7300 with primers targeting CYR61 and ANKRD1: CYR61 (forward: 5′-AGCCTCGCATCCTATACAACC-3′; reverse: 5′-TTCTTTCACAAGGCGGCACTC-3′) and ANKRD (forward: 5′-GTGTAGCACCAGATCCATCG-3′; reverse: 5′-CGGTGAGACTGAACCGCTAT-3′). The gene expression was normalized to glyceraldehyde-3-phosphate dehydrogenase.

RNA-seq and bioinformatics analysis

Total RNAs were extracted by TRIzol (Thermo Fisher Scientific) from SEMA3A-treated U87-MG cells and control cells. Three replicates for each sample were prepared and analyzed. The resulting RNAs were then used to prepare libraries using the Illumina TruSeq Stranded mRNA Library Prep Kit set A (Illumina, RS-122-2101) or set B (Illumina, RS-122-2102). The libraries were sequenced using Illumina HiSeq 4000 (paired-end, 50 base pairs).

Reads were aligned to the hg19 reference genome using STAR (*46*). Only uniquely mapped reads were kept for further analysis. The number of reads for each gene was counted using htseq-count 33 according to GENCODE human annotation release 24. Differentially expressed genes were identified with DESeq2 (*47*). Genes that are not expressed (sum of counts ≤ 1 across all samples) were removed

before differential gene expression analysis. Two sets of analyses were performed to identify differentially expressed genes. Genes with adjusted *P* value of <0.1 were considered as differentially expressed.

To identify differentially expressed genes under different combinations between condition and genotype, a DESeq2 model with four groups (two genotypes and two conditions) was built and each pair of conditions was compared separately to identify differentially expressed genes. To identify genes with differential effects upon SEMA3 treatment under WT and LATS1/2 KO genotypes, a model—consisting of the genotypes, the conditions (SEMA3 versus control), and an interaction term—was built with DESeq2 and the interaction term was tested to determine the SEMA3 effect under the two genotypes. In both cases, genes with adjusted *P* value of <0.1 were considered as differentially expressed. Enrichment analysis of differentially expressed genes was performed using Metascape (*48*).

TurboID

Proximal proteins of PLXNA1 were biotinylated and isolated using the TurboID methods (*49*) with a few modifications. Briefly, U87 cells were infected with lentivirus expressing PlexinA1-TurboID–fused protein or Vector-TurboID as control, and a stable population was selected, respectively. The medium was supplemented with biotin at 1 μM for 15 min before harvest. Cells were washed three times on ice with cold PBS and lysed in radioimmunoprecipitation assay (RIPA) lysis buffer [150 mM NaCl, 50 mM tris (pH 7.5), 1% NP-40, 0.5% sodium deoxycholate, and 0.1% SDS]. Affinity purification was done with streptavidin-coated magnetic beads (20 μl of slurry per 100-mm dish of cells; Thermo Fisher Scientific, #88817).

Protein samples on magnetic beads were subsequently washed twice with 1 ml of RIPA lysis buffer, once with 1 ml of 2% SDS, once with 1 ml of 1 M KCl, once with 1 ml of 0.1 M Na_2CO_3, and twice with 1 ml of 2 M urea in 50 mM tris-HCl (pH 7.5). These beads were incubated with 150 μl of 2 M urea/50 mM tris containing 1 mM dithiothreitol and 1 μg of sequencing grade trypsin (Promega, #V5111) overnight at 37°C with shaking. Digested samples were acidified using trifluoroacetic acid to a final concentration of 0.5%. Peptide samples were desalted on C18 Sep-Pak cartridges (Waters) and evaporated to dryness in a vacuum concentrator.

TMT labeling and LC-MS/MS

Each peptide sample was resuspended with 20 μl of 25 mM phosphate buffer (pH 8.0) and labeled with different isobaric TMT reagent (8 μl × 5 μg/μl; Thermo Fisher Scientific, #90110) for 2 hours at room temperature. These labeled peptides were then combined and desalted on C18 spin columns and evaporated to dryness in a vacuum concentrator. These combined peptide samples were first fractionated using a HILIC column (TSKgel Amide-80) to generate 14 fractions. Fractions were combined into five and then analyzed by LC-MS/MS on the Thermo Orbitrap Fusion MS system. MS data were analyzed via the COMET peptide search engine as part of the Trans-Proteomic Pipeline (TPP). The search results were then processed using TPP, where quantification of the TMT reporter ion was analyzed by the Libra software tool. A false discovery rate of less than 1% was applied for the peptide identification, and a minimum intensity of the TMT reporter ion was set at 1000.

Shear stress

HEK293A cells were seeded onto poly-L-ornithine [0.001% (w/v)]–coated glass slides and grown until confluence. For the shear experiments, the slides were assembled into rectangular parallel plate flow chambers and connected to a diaphragm liquid pump (KNF, FF 12KPDCB-4) controlled by a custom pump controller. HEK293A cells were exposed to shear stress (τ) of 1.0 ± 0.5 dyn/cm^2 or kept as static control in the chamber. Shear stress in the chamber occurs via Poiseuille flow through a rectangular cross section, which obeys the relationship: $\tau = \frac{6Q\mu}{wh^2}$, where flow rate ($Q$) is 13.5 ml/min, viscosity (μ) is approximately 1 cP, channel height (h) is 0.79 mm, and channel width (w) is 19.37 mm. The system was kept in a humidified incubator at 37°C, and the circulating medium was equilibrated with humidified 5% (v/v) CO_2.

RhoA and Rac1 activation assay

The RhoA and Rac1 activation assays were performed by measuring the active RhoA/Rac1 interacting with Rho-GTP–binding strips using G-LISA kits (Cytoskeleton Inc. #BK124 and #BK127). Briefly, 25 μg of cell lysates of each group was incubated with Rho-GTP–binding strips at 4°C for 30 min with shaking. GTP-bound RhoA or Rac1 in cell lysates was bound to the wells, while GDP-bound GTPase was removed during washing steps. The active GTPase was detected with a protein-specific antibody, followed by incubation with horseradish peroxidase (HRP)–linked secondary antibody and HRP detection reagent. The signal was read by measuring the absorbance at 490 nm using a microplate spectrophotometer (Infinite 200 Pro, TECAN).

SUPPLEMENTARY MATERIALS

Supplementary material for this article is available at https://science.org/doi/10.1126/sciadv.abl9806

View/request a protocol for this paper from *Bio-protocol*.

REFERENCES AND NOTES

1. T. Worzfeld, S. Offermanns, Semaphorins and plexins as therapeutic targets. *Nat. Rev. Drug Discov.* **13**, 603–621 (2014).
2. M. Rehman, L. Tamagnone, Semaphorins in cancer: Biological mechanisms and therapeutic approaches. *Semin. Cell Dev. Biol.* **24**, 179–189 (2013).
3. R. P. Kruger, J. Aurandt, K. L. Guan, Semaphorins command cells to move. *Nat. Rev. Mol. Cell Biol.* **6**, 789–800 (2005).
4. E. Castro-Rivera, S. Ran, R. A. Brekken, J. D. Minna, Semaphorin 3B inhibits the phosphatidylinositol 3-kinase/Akt pathway through neuropilin-1 in lung and breast cancer cells. *Cancer Res.* **68**, 8295–8303 (2008).
5. T. Kuroki, F. Trapasso, S. Yendamuri, A. Matsuyama, H. Alder, N. N. Williams, L. R. Kaiser, C. M. Croce, Allelic loss on chromosome 3p21.3 and promoter hypermethylation of semaphorin 3B in non-small cell lung cancer. *Cancer Res.* **63**, 3352–3355 (2003).
6. V. I. Loginov, A. A. Dmitriev, V. N. Senchenko, I. V. Pronina, D. S. Khodyrev, A. V. Kudryavtseva, G. S. Krasnov, G. V. Gerashchenko, L. I. Chashchina, T. P. Kazubskaya, T. T. Kondratieva, M. I. Lerman, D. Angeloni, E. A. Braga, V. I. Kashuba, Tumor suppressor function of the SEMA3B gene in human lung and renal cancers. *PLOS ONE* **10**, e0123369 (2015).
7. P. Shahi, C. Y. Wang, J. Chou, C. Hagerling, H. Gonzalez Velozo, A. Ruderisch, Y. Yu, M. D. Lai, Z. Werb, GATA3 targets semaphorin 3B in mammary epithelial cells to suppress breast cancer progression and metastasis. *Oncogene* **36**, 5567–5575 (2017).
8. S. Ma, Z. Meng, R. Chen, K. L. Guan, The hippo pathway: Biology and pathophysiology. *Annu. Rev. Biochem.* **88**, 577–604 (2019).
9. D. Pan, The hippo signaling pathway in development and cancer. *Dev. Cell* **19**, 491–505 (2010).
10. Z. Meng, T. Moroishi, K. L. Guan, Mechanisms of hippo pathway regulation. *Genes Dev.* **30**, 1–17 (2016).
11. Z. Meng, Y. Qiu, K. C. Lin, A. Kumar, J. K. Placone, C. Fang, K. C. Wang, S. Lu, M. Pan, A. W. Hong, T. Moroishi, M. Luo, S. W. Plouffe, Y. Diao, Z. Ye, H. W. Park, X. Wang, F. X. Yu, S. Chien, C. Y. Wang, B. Ren, A. J. Engler, K. L. Guan, RAP2 mediates mechanoresponses of the Hippo pathway. *Nature* **560**, 655–660 (2018).
12. H. W. Park, Y. C. Kim, B. Yu, T. Moroishi, J. S. Mo, S. W. Plouffe, Z. Meng, K. C. Lin, F. X. Yu, C. M. Alexander, C. Y. Wang, K. L. Guan, Alternative Wnt signaling activates YAP/TAZ. *Cell* **162**, 780–794 (2015).

13. F. Sanchez-Vega, M. Mina, J. Armenia, W. K. Chatila, A. Luna, K. C. La, S. Dimitriadoy, D. L. Liu, H. S. Kantheti, S. Saghafinia, D. Chakravarty, F. Daian, Q. Gao, M. H. Bailey, W.-W. Liang, S. M. Foltz, I. Shmulevich, L. Ding, Z. Heins, A. Ochoa, B. Gross, J. Gao, H. Zhang, R. Kundra, C. Kandoth, I. Bahceci, L. Dervishi, U. Dogrusoz, W. Zhou, H. Shen, P. W. Laird, G. P. Way, C. S. Greene, H. Liang, Y. Xiao, C. Wang, A. Iavarone, A. H. Berger, T. G. Bivona, A. J. Lazar, G. D. Hammer, T. Giordano, L. N. Kwong, G. M. Arthur, C. Huang, A. D. Tward, M. J. Frederick, F. M. Cormick, M. Meyerson; Cancer Genome Atlas Research Network, E. M. Van Allen, A. D. Cherniack, G. Ciriello, C. Sander, N. Schultz, Oncogenic signaling pathways in the cancer genome atlas. *Cell* **173**, 321, 337.e10 (2018).
14. F. X. Yu, B. Zhao, K. L. Guan, Hippo pathway in organ size control, tissue homeostasis, and cancer. *Cell* **163**, 811–828 (2015).
15. I. M. Moya, G. Halder, Hippo-YAP/TAZ signalling in organ regeneration and regenerative medicine. *Nat. Rev. Mol. Cell Biol.* **20**, 211–226 (2019).
16. Y. Tomizawa, Y. Sekido, M. Kondo, B. Gao, J. Yokota, J. Roche, H. Drabkin, M. I. Lerman, A. F. Gazdar, J. D. Minna, Inhibition of lung cancer cell growth and induction of apoptosis after reexpression of 3p21.3 candidate tumor suppressor gene SEMA3B. *Proc. Natl. Acad. Sci. U.S.A.* **98**, 13954–13959 (2001).
17. Y. Sekido, S. Bader, F. Latif, J. Y. Chen, F. M. Duh, M. H. Wei, J. P. Albanesi, C. C. Lee, M. I. Lerman, J. D. Minna, Human semaphorins A(V) and IV reside in the 3p21.3 small cell lung cancer deletion region and demonstrate distinct expression patterns. *Proc. Natl. Acad. Sci. U.S.A.* **93**, 4120–4125 (1996).
18. M. Ito, G. Ito, M. Kondo, M. Uchiyama, T. Fukui, S. Mori, H. Yoshioka, Y. Ueda, K. Shimokata, Y. Sekido, Frequent inactivation of RASSF1A, BLU, and SEMA3B on 3p21.3 by promoter hypermethylation and allele loss in non-small cell lung cancer. *Cancer Lett.* **225**, 131–139 (2005).
19. I. Tischoff, A. Markwarth, H. Witzigmann, D. Uhlmann, J. Hauss, A. Mirmohammadsadegh, C. Wittekind, U. R. Hengge, A. Tannapfel, Allele loss and epigenetic inactivation of 3p21.3 in malignant liver tumors. *Int. J. Cancer* **115**, 684–689 (2005).
20. Z. Meng, T. Moroishi, V. Mottier-Pavie, S. W. Plouffe, C. G. Hansen, A. W. Hong, H. W. Park, J. S. Mo, W. Lu, S. Lu, F. Flores, F. X. Yu, G. Halder, K. L. Guan, MAP4K family kinases act in parallel to MST1/2 to activate LATS1/2 in the Hippo pathway. *Nat. Commun.* **6**, 8357 (2015).
21. R. El Masri, J. Delon, RHO GTPases: From new partners to complex immune syndromes. *Nat. Rev. Immunol.* **21**, 499–513 (2021).
22. A. Hergovich, The roles of NDR protein kinases in hippo signalling. *Genes (Basel)* **7**, 21 (2016).
23. S. Kaneko, X. Chen, P. Lu, X. Yao, T. G. Wright, M. Rajurkar, K. I. Kariya, J. Mao, Y. T. Ip, L. Xu, Smad inhibition by the Ste20 kinase Misshapen. *Proc. Natl. Acad. Sci. U.S.A.* **108**, 11127–11132 (2011).
24. T. Mahmoudi, V. S. W. Li, S. S. Ng, N. Taouatas, R. G. J. Vries, S. Mohammed, A. J. Heck, H. Clevers, The kinase TNIK is an essential activator of Wnt target genes. *EMBO J.* **28**, 3329–3340 (2009).
25. A. Varshavsky, O. Kessler, S. Abramovitch, B. Kigel, S. Zaffryar, G. Akiri, G. Neufeld, Semaphorin-3B is an angiogenesis inhibitor that is inactivated by furin-like pro-protein convertases. *Cancer Res.* **68**, 6922–6931 (2008).
26. K. L. DeCicco-Skinner, G. H. Henry, C. Cataisson, T. Tabib, J. C. Gwilliam, N. J. Watson, E. M. Bullwinkle, L. Falkenburg, R. C. O'Neill, A. Morin, J. S. Wiest, Endothelial cell tube formation assay for the in vitro study of angiogenesis. *J. Vis. Exp.* e51312 (2014).
27. K. Yuan, M. E. Orcholski, N. F. Huang, V. A. de Jesus Perez, In vivo study of human endothelial-pericyte interaction using the matrix gel plug assay in mouse. *J. Vis. Exp.* 54617 (2016).
28. Y. Wang, H. He, N. Srivastava, S. Vikarunnessa, Y.-b. Chen, J. Jiang, C. W. Cowan, X. Zhang, Plexins are GTPase-activating proteins for Rap and are activated by induced dimerization. *Sci. Signal.* **5**, ra6 (2012).
29. X. Chen, A. C. E. Shibata, A. Hendi, M. Kurashina, E. Fortes, N. L. Weilinger, B. A. M. Vicar, H. Murakoshi, K. Mizumoto, Rap2 and TNIK control plexin-dependent tiled synaptic innervation in C. elegans. *eLife* **7**, e38801 (2018).
30. K. F. Cho, T. C. Branon, N. D. Udeshi, S. A. Myers, S. A. Carr, A. Y. Ting, Proximity labeling in mammalian cells with TurboID and split-TurboID. *Nat. Protoc.* **15**, 3971–3999 (2020).
31. A. L. Stiegler, T. J. Boggon, The N-terminal GTPase domain of p190RhoGAP proteins is a PseudoGTPase. *Structure* **26**, 1451–1461.e4 (2018).
32. S. R. Frank, C. P. Köllmann, P. Luong, G. G. Galli, L. Zou, A. Bernards, G. Getz, R. A. Calogero, M. Frödin, S. H. Hansen, p190 RhoGAP promotes contact inhibition in epithelial cells by repressing YAP activity. *J. Cell Biol.* **217**, 3183–3201 (2018).
33. K. Wennerberg, M. A. Forget, S. M. Ellerbroek, W. T. Arthur, K. Burridge, J. Settleman, C. J. der, S. H. Hansen, Rnd proteins function as RhoA antagonists by activating p190 RhoGAP. *Curr. Biol.* **13**, 1106–1115 (2003).
34. I. Oinuma, K. Kawada, K. Tsukagoshi, M. Negishi, Rnd1 and Rnd3 targeting to lipid raft is required for p190 RhoGAP activation. *Mol. Biol. Cell* **23**, 1593–1604 (2012).
35. S. M. Zanata, I. Hovatta, B. Rohm, A. W. Puschel, Antagonistic effects of Rnd1 and RhoD GTPases regulate receptor activity in Semaphorin 3A-induced cytoskeletal collapse. *J. Neurosci.* **22**, 471–477 (2002).
36. B. Rohm, B. Rahim, B. Kleiber, I. Hovatta, A. W. Puschel, The semaphorin 3A receptor may directly regulate the activity of small GTPases. *FEBS Lett.* **486**, 68–72 (2000).
37. T. Okada, S. Sinha, I. Esposito, G. Schiavon, M. A. López-Lago, W. Su, C. A. Pratilas, C. Abele, J. M. Hernandez, M. Ohara, M. Okada, A. Viale, A. Heguy, N. D. Socci, A. Sapino, V. E. Seshan, S. Long, G. Inghirami, N. Rosen, F. G. Giancotti, The Rho GTPase Rnd1 suppresses mammary tumorigenesis and EMT by restraining Ras-MAPK signalling. *Nat. Cell Biol.* **17**, 81–94 (2015).
38. B. Zhao, X. Wei, W. Li, R. S. Udan, Q. Yang, J. Kim, J. Xie, T. Ikenoue, J. Yu, L. Li, P. Zheng, K. Ye, A. Chinnaiyan, G. Halder, Z. C. Lai, K. L. Guan, Inactivation of YAP oncoprotein by the Hippo pathway is involved in cell contact inhibition and tissue growth control. *Genes Dev.* **21**, 2747–2761 (2007).
39. V. Mehta, K. L. Pang, D. Rozbesky, K. Nather, A. Keen, D. Lachowski, Y. Kong, D. Karia, M. Ameismeier, J. Huang, Y. Fang, A. del Rio Hernandez, J. S. Reader, E. Y. Jones, E. Tzima, The guidance receptor plexin D1 is a mechanosensor in endothelial cells. *Nature* **578**, 290–295 (2020).
40. C. Jiang, A. Javed, L. Kaiser, M. M. Nava, R. Xu, D. T. Brandt, D. Zhao, B. Mayer, J. Fernández-Baldovinos, L. Zhou, C. Höß, K. Sawmynaden, A. Oleksy, D. Matthews, L. S. Weinstein, H. Hahn, H. J. Gröne, P. L. Graumann, C. M. Niessen, S. Offermanns, S. A. Wickström, T. Worzfeld, Mechanochemical control of epidermal stem cell divisions by B-plexins. *Nat. Commun.* **12**, 1308 (2021).
41. Y. Huang, R. Tejero, V. K. Lee, C. Brusco, T. Hannah, T. B. Bertucci, C. Junqueira Alves, I. Katsyv, M. Kluge, R. Foty, B. Zhang, C. C. Friedel, G. Dai, H. Zou, R. H. Friedel, Plexin-B2 facilitates glioblastoma infiltration by modulating cell biomechanics. *Commun. Biol.* **4**, 145 (2021).
42. L. Wang, J. Y. Luo, B. Li, X. Y. Tian, L. J. Chen, Y. Huang, J. Liu, D. Deng, C. W. Lau, S. Wan, D. Ai, K. L. K. Mak, K. K. Tong, K. M. Kwan, N. Wang, J. J. Chiu, Y. Zhu, Y. Huang, Integrin-YAP/TAZ-JNK cascade mediates atheroprotective effect of unidirectional shear flow. *Nature* **540**, 579–582 (2016).
43. A. L. Elaimy, A. M. Mercurio, Convergence of VEGF and YAP/TAZ signaling: Implications for angiogenesis and cancer biology. *Sci. Signal.* **11**, (2018).
44. A. L. Stiegler, T. J. Boggon, p190RhoGAP proteins contain pseudoGTPase domains. *Nat. Commun.* **8**, 506 (2017).
45. P. Kastana, F. T. Zahra, D. Ntenekou, S. K.-Pavlou, D. Beis, M. S. Lionakis, C. M. Mikelis, E. Papadimitriou, Matrigel plug assay for in vivo evaluation of angiogenesis. *Methods Mol. Biol.* **1952**, 219–232 (2019).
46. A. Dobin, C. A. Davis, F. Schlesinger, J. Drenkow, C. Zaleski, S. Jha, P. Batut, M. Chaisson, T. R. Gingeras, STAR: Ultrafast universal RNA-seq aligner. *Bioinformatics* **29**, 15–21 (2013).
47. M. I. Love, W. Huber, S. Anders, Moderated estimation of fold change and dispersion for RNA-seq data with DESeq2. *Genome Biol.* **15**, 550 (2014).
48. Y. Zhou, B. Zhou, L. Pache, M. Chang, A. H. Khodabakhshi, O. Tanaseichuk, C. Benner, S. K. Chanda, Metascape provides a biologist-oriented resource for the analysis of systems-level datasets. *Nat. Commun.* **10**, 1523 (2019).
49. T. C. Branon, J. A. Bosch, A. D. Sanchez, N. D. Udeshi, T. Svinkina, S. A. Carr, J. L. Feldman, N. Perrimon, A. Y. Ting, Efficient proximity labeling in living cells and organisms with TurboID. *Nat. Biotechnol.* **36**, 880–887 (2018).

Acknowledgments: We thank Y. Zou at University of California, San Diego for suggestions on experiment design. We also appreciate the support from other colleagues in Z.M. and K.-L.G.'s laboratories. **Funding:** Z.M. is supported by the National Institute of General Medical Sciences of the National Institutes of Health (NIH) under award number R35GM142504. This project is also, in part, supported by a grant from the Elsa U. Pardee Foundation to Z.M. K.-L.G. is supported by NIH grants R35CA196878, R01CA268179, and R01GM51586. F.G.G. is supported by NIH R01 CA191222 and R35 CA197566. A.J.E. is supported by NIH grants R01CA206880 and R21CA217735 and National Science Foundation grant 1763139. B.Y. is supported by an NIH training grant T32CA009523. **Author contributions:** Z.M., F.-L.L., and K.-L.G. conceived the project and wrote the manuscript. Z.M., F.-L.L., C.F., B.Y., Y.W., K.C.L., D.Y., M.L., and V.F. performed the experiments. Y.Q., X.C., X.M., Y.D., and B.R. performed the bioinformatics analyses. F.G.G. and A.J.E. assisted in experimental design and data analyses. **Competing interests:** K.-L.G. is a cofounder of Vivace Therapeutics and has an equity interest in Vivace. All other authors declare that they have no competing interests. **Data and materials availability:** All data needed to evaluate the conclusions in the paper are present in the paper and/or the Supplementary Materials. The source data for the graph representations can be found in the online version of the paper. The RNA-seq data are available in GEO DataSets with the accession number GSE139630 (token: mhanmqeivtmhtir).

Submitted 17 August 2021
Accepted 11 April 2022
Published 25 May 2022
10.1126/sciadv.abl9806